Polymer 50 (2009) 2149–2153

Contents lists available at ScienceDirect

Polymer

journal homepage: www.elsevier.com/locate/polymer

Crystallization-induced order in polystyrene-poly(ethylene oxide) metallo-supramolecular diblock copolymer

Mahmoud Al-Hussein [a,*], Wim H. de Jeu [b,c,1]

[a] Department of Physics, University of Jordan, Amman 11942, Jordan
[b] FOM-Institute for Atomic and Molecular Physics, Kruislaan 407, 1098 SJ Amsterdam, The Netherlands
[c] Department of Chemical Engineering and Chemistry, Eindhoven University of Technology, 5600 MB Eindhoven, The Netherlands

ARTICLE INFO

Article history:
Received 30 December 2008
Received in revised form
12 February 2009
Accepted 6 March 2009
Available online 13 March 2009

Keywords:
Metallo diblock copolymers
Crystallization
X-ray scattering

ABSTRACT

The solid-state morphology of polystyrene-poly(ethylene oxide) metallo-supramolecular diblock copolymer PS_{20}-[Ru]-PEO_{70}, has been investigated by small-and wide-angle X-ray scattering and atomic force microscopy. Above the melting point of PEO the metal–ligand complexes and their associated counter ions are known to form aggregates within the still disordered polymer matrix of PS and PEO. Crystallization of PEO induces microphase separation between the PS and the PEO blocks. In addition, the metal–ligand aggregates are forced out of the crystalline PEO part and subsequently order at the interface in the amorphous PS block into a (short-range) square lattice.

1. Introduction

Over the past decades, substantial progress has been made toward the generation of supramolecular copolymers as a result of the discovery of new synthetic methods such as the ring-opening polymerization and the metal-catalyzed polycondensation [1]. Using these methods, mutually repulsive chemical moieties can be connected by physical supramolecular interactions (hydrogen bonds, metal ion coordination, or electrostatic interactions) to form block copolymer-like supramolecules [2–4]. The resulting materials hold the potential to generate spatially organized functional structures on the nanoscale desirable for new electronic and electro-optic devices. Among these supramolecular copolymers, the metal-based copolymers are emerging as interesting candidates to generate novel hybrid metal/polymer composite materials via the self-assembly approach [5,6].

In the recently synthesized metallo-supramolecular diblock copolymers, a metal–ligand complex (MLC) is used as a supramolecular linker between two different polymer chains as opposed to the commonly used covalent bond in conventional diblock copolymers [7]. Conventional diblock copolymers have gained their importance from their ability to self-assemble into a series of periodic microdomains with a 10–100 nm period depending on both the strength of the repulsive interaction between the two blocks and their composition [8–11]. The resulting morphologies include lamellae, hexagonally packed cylinders, cubically arranged spheres and bicontinuous structures. The geometry of these domains is largely determined by the balance between the enthalpy associated with the domain interfaces and the stretching entropy associated with the microphase separation. In the case of metallo-supramolecular copolymers, the MLC's are an integral part of the polymer chains and their self-organization provides an additional tool to influence the final morphology. Such ideas of combining interactions in the design of new synthetic macromolecular materials might hold the key to the development of new self-assembled nanostructures over many length scales needed for advanced technologies [12].

In previous work we reported the effect of the MLC's on the melt phase behavior of a metallo-supramolecular diblock copolymers, namely polystyrene-[Ru]-poly(ethylene oxide) or PS_{20}-[Ru]-PEO_{70}. (see Fig. 1) in the presence of different counter ions [13,14]. In the case of hexafluorophosphate counter anions (PF_6^-), a quantitative analysis of the small-angle X-ray scattering (SAXS) in the melt indicated that the MLC's and their associated counter ions tend to form aggregates within the polymer matrix. A liquidlike model of spherical ion-counter ion aggregates (radius ~1.5 nm) surrounded by a polymer shell (radius ~2.4 nm) fitted the single broad peak characteristic of the SAXS well [13]. Long annealing in the melt

* Corresponding author.
E-mail addresses: m.alhussein@ju.edu.jo (M. Al-Hussein), dejeu@mail.pse.umass.edu (W.H. de Jeu).
[1] Present address: Polymer Science and Engineering, University of Massachusetts, 120 Governors Drive, Amherst, MA 01003, USA.

0032-3861/$ – see front matter © 2009 Elsevier Ltd. All rights reserved.
doi:10.1016/j.polymer.2009.03.004

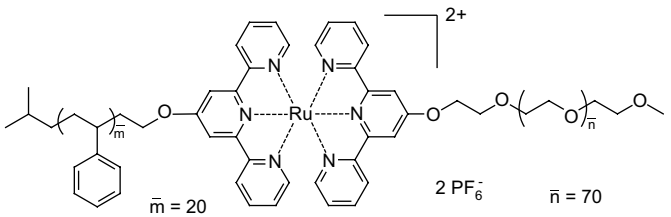

Fig. 1. Structure of the PS_{20}-[Ru]-PEO_{70} block copolymer. The numbers in the subscript indicate the degree of polymerization.

produced essentially no changes in the morphology. In the solid state, however, crystallization of the PEO block provides an additional driving force toward structure formation. As crystallization is a strong phase transition, it plays a prominent role in determining the final morphology of conventional block copolymers. In this study, we report time- and temperature-resolved small- and wide-angle X-ray scattering together with atomic force microscopy measurements of the solid-state morphology of PS_{20}-[Ru]-PEO_{70}. The results indicate crystallization-induced microphase separation of the PS and PEO blocks. In addition, the MLC aggregates are pushed out of the crystalline region, which leads to the formation of an ordered ligand structure.

2. Experimental

2.1. Samples

Fig. 1 shows the chemical structure of the PS_{20}-[Ru]-PEO_{70} copolymer used with the PEO and PS blocks connected via a bis(terpyridine)ruthenium(II) ion complex. The synthesis of the system has been described in detail elsewhere [15]. The copolymer has a polydispersity of 1.10. Using the bulk density of bis(terpyridine)ruthenium with the two PF_6^- counter ions and that of PS and PEO, the volume fractions of the MLC, PS and PEO have been calculated as 15.8, 35.1, and 49.1%, respectively [14].

2.2. Small- and wide-angle X-ray scattering (SAXS/WAXS)

Time-dependent SAXS and WAXS were performed in transmission geometry to probe the morphology development during the crystallization process. These were conducted using an in-house setup at the FOM-Institute for Atomic and Molecular Physics in Amsterdam (The Netherlands) with a rotating anode X-ray generator (Rigaku RA-H300) operating at 18 kW. By employing two parabolic multilayer mirrors (Bruker, Karlsruhe), a highly parallel beam (divergence about 25 mdeg) of a monochromatic CuK_α radiation ($\lambda = 0.154$ nm) was obtained. A Linkam CSS450 cell was used as a temperature-controlled sample stage. A small amount of the copolymer powder was placed in a brass washer with a diameter of 5 mm and thickness of 1 mm and sealed with two kapton foils. All samples were heated to well above the melting point of PEO at about 60 °C and subsequently cooled down to the desired crystallization temperature, T_c. A counting time of 10 min was used for each scan.

The SAXS patterns were recorded with a Bruker Hi-Star area detector at a sample-to-detector distance of 1.03 m. The two-dimensional scattering patterns were radially integrated, corrected for background, and subsequently displayed as one-dimensional plots of the intensity as a function of $q = (4\pi/\lambda)\sin\ \theta$, the modulus of the scattering vector q, in which 2θ is the scattering angle. The WAXS curves were recorded using a linear position detector (M. Braun, Germany).

2.3. Atomic force microscopy (AFM)

Fresh surfaces representing the bulk morphology were obtained from crystallized samples using a homemade cryogenic microtome. The samples were first isothermally crystallized in a 2 mm diameter hole in a Teflon tape and subsequently cooled using liquid nitrogen and cut. By choosing the right temperature (between too brittle and too soft), a surface can be obtained that is typical of the bulk morphology [16] ("poor man's TEM"). The resulting surface was investigated at room temperature using a Solver AFM (NT-MDT, Zelenograd, Moscow) in the tapping mode. A standard cantilever with a resonant frequency of about 300 kHz and a silicon tip with a radius of curvature of 10 nm were used.

3. Results

3.1. Isothermal crystallization

Fig. 2a and b show SAXS and WAXS curves obtained at different times during the isothermal crystallization at $T_c = 30$ °C, respectively. The SAXS curves indicate that in the first 1300 min, a single broad peak (indicated as q_m^*) characteristic of the melt [13,14] maintains its appearance with almost no changes in either intensity

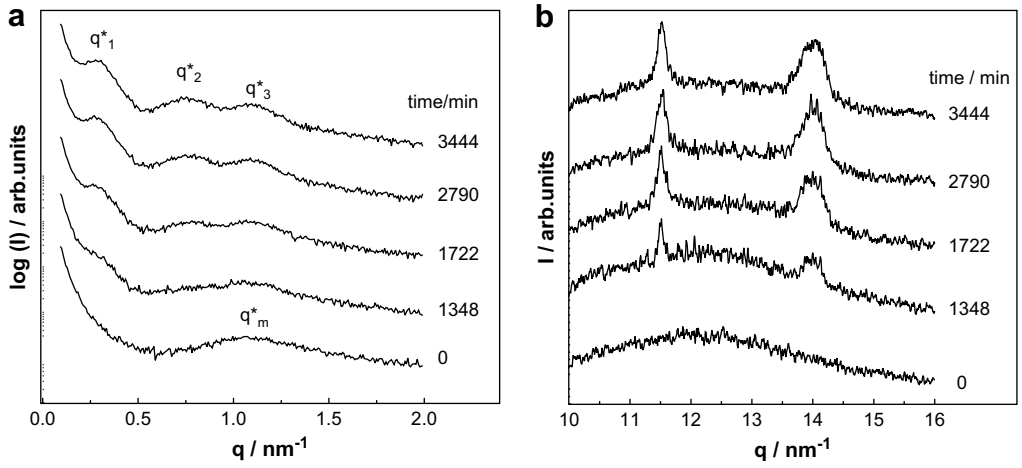

Fig. 2. SAXS (a) and WAXS intensity (b) data during an isothermal crystallization at $T_c = 30$ °C.

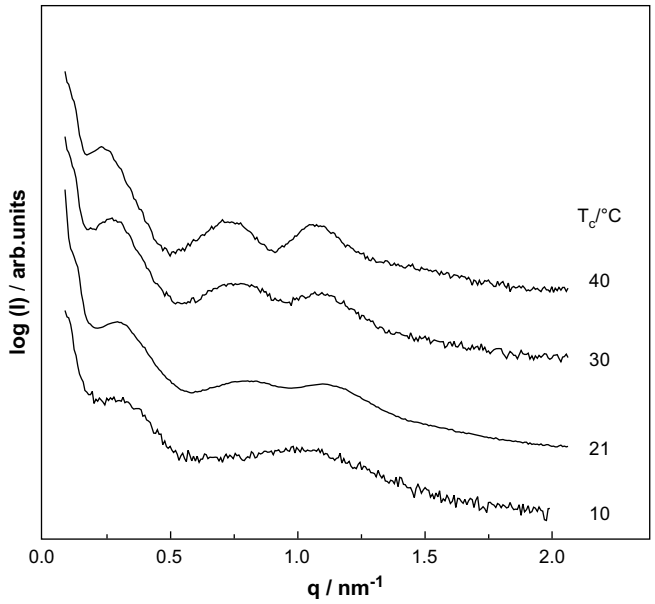

Fig. 3. SAXS curves after saturation for samples isothermally crystallized at the indicated temperatures.

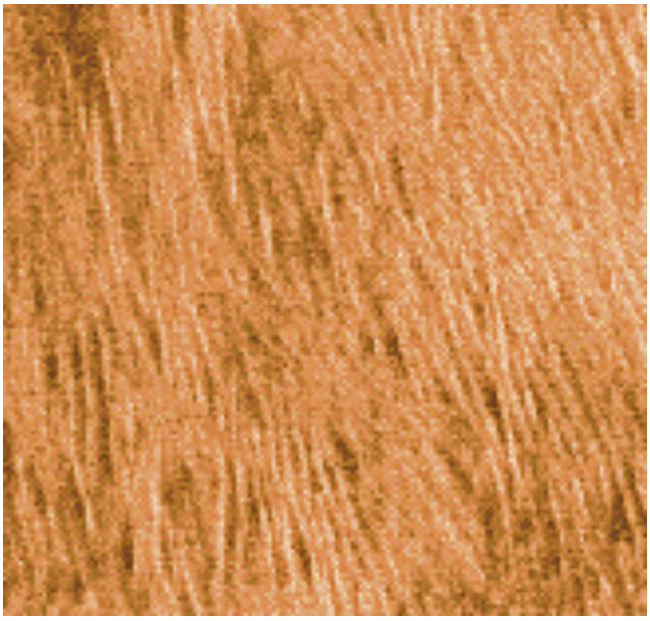

Fig. 4. AFM phase image of a microtomed surface of a sample isothermally crystallized at $T_c = 21$ °C (area 1×1 μm^2).

or position. After this time two new peaks occur at lower q values designated by q_1^* and q_2^*, respectively. The intensities of these peaks grow with the crystallization time until saturation occurs. First q_1^* seems to develop independently while somewhat later q_m^* appears to split into q_2^* and q_3^*. The increase in intensity at q_2^*, and q_3^* becomes more noticeable at later stages of the crystallization process. The development of the new SAXS peaks is accompanied by the appearance of two peaks in the corresponding WAXS intensity at $q = 11.52$ nm^{-1} and $q = 13.99$ nm^{-1}, respectively. These positions coincide with those of the (120) and (032 + 112) reflections of PEO homopolymer [17]. The results indicate that the crystallinity increases as a function of the crystallization time. Evidently any possible order of the MLCs after crystallization does not lead to additional reflections in the WAXS region. Fig. 3 shows the final saturated SAXS curves at long times for samples isothermally crystallized at different temperatures. These results are summarized in Table 1, in which also the full width at half maximum (FWHM) of the peak at q_2^* is given. For samples crystallized at temperatures >20 °C, all three peaks are well resolved, but for crystallization at 10 °C the peaks at q_2^* and q_3^* cannot be distinguished. Note that for all samples crystallized at $T_c > 20$ °C, we observe $q_3^* = q_2^*\sqrt{2}$ even though the absolute positions vary with temperature.

Finally, direct space images of the bulk morphology were obtained by AFM of microtomed surfaces as described in Section 2.3. Fig. 4 gives a typical example from a sample crystallized at $T_c = 21$ °C in which continuously alternating crystalline lamellae with different orientations can be clearly distinguished. The interlamellar period as estimated from the AFM image is about 21 nm.

Table 1
Positions of the SAXS peaks of Fig. 3, together with their corresponding Bragg periods. For q_2^* also the FWHM Δq_2 and the domain size/correlation length $L = 2\pi/\Delta q_2$ are given. q_1^* values are obtained after performing the Lorentz correction.

T_c/°C	q_1^*/nm^{-1}	q_2^*/nm^{-1}	q_3^*/nm^{-1}	d_1/nm	d_2/nm	peak q_2^*	
						Δq_2/nm^{-1}	L/nm
10	0.33	–	–	19.0	–	–	–
21	0.29	0.79	1.12	21.7	7.95	0.22	28
30	0.27	0.76	1.08	23.3	8.27	0.21	30
40	0.23	0.74	1.06	27.3	8.49	0.19	34

3.2. Thermal stability

Temperature-dependent SAXS measurements were performed to asses the thermal stability of the isothermally crystallized samples. Fig. 5a shows as a typical example a series of SAXS curves of a sample crystallized at $T_c = 30$ °C taken during subsequent heating to the melt. The intensity of the peaks at q_1^* and q_2^* drops substantially at 48 °C, and at 50 °C only the broad peak of the melt (q_m^*) is left. Interestingly, for samples crystallized at $T_c = 10$ °C (Fig. 5b), the peaks at q_2^*, and q_3^* (that initially could not be distinguished) become resolved at temperatures above 30 °C. They gain intensity during further heating to 45 °C before disappearing at 50 °C. Finally again only the broad peak of the melt is retained, similar to the case of Fig. 5a. These results clearly indicate that the splitting of the broad bump from the melt (q_m^*) into the peaks at q_2^* and q_3^* is directly related to the crystallization of the PEO as revealed by q_1^*.

4. Discussion

The solid-state morphology of conventional diblock copolymers containing crystallizable blocks is known to be significantly influenced by the crystallization conditions (see for reviews Refs. [9,18]). The final morphology can be either dominated by crystallization or by the initial block copolymer morphology, depending on the relative positions of T_c of the crystallizable block, the glass transition temperature of the amorphous block (T_g), and the block copolymer order–disorder transition temperature (T_{ODT}). In addition, the final morphology can be influenced by the kinetics of the various processes [16,19–23]. In particular crystallization can induce microphase separation in an otherwise mixed block copolymer system. In our system, the PEO and PS blocks are still mixed like in the corresponding diblock copolymer without the MLC [13]. However, as reported earlier, inside this polymer mixture the MLC's

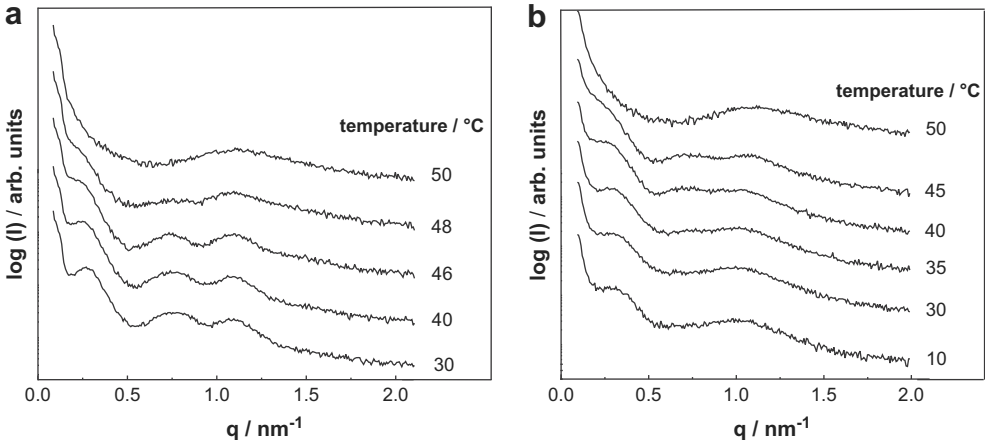

Fig. 5. SAXS curves during heating of a sample isothermally crystallized at $T_c = 30\,^{\circ}C$ (a) and $T_c = 10\,^{\circ}C$ (b).

are segregated into spherical aggregates of the order of a few nanometers as revealed by the broad bump at q_m^* [13].

The experimental results provide unequivocal evidence for crystallization of the PEO block. WAXS confirms essentially the same crystalline structure as for a PEO homopolymer: a monoclinic lattice with unit cell parameters $a = 0.805$ nm, $b = 1.304$ nm, $c = 1.948$ nm and $\beta = 125.4$ [24]. The AFM images show typical crystalline lamellae, continuous and alternating with somewhat thicker amorphous regions. From these observations we conclude that crystallization induces microphase separation between the PS and PEO blocks. As in all samples the X-ray peak at q_1^* is observed only below the melting point of PEO, we attribute q_1^* to this phase separation. Calculating the ratios q_2^*/q_1^* and q_3^*/q_1^* from the data in Table 1 clearly shows that neither q_2^* nor q_3^* can be connected in a simple way to q_1^*. The period of 20 nm corresponding to q_1^* is rather large and increases with crystallization temperature. This value comes close to the interlamellar period estimated from AFM (about 21 nm at $T_c = 21\,^{\circ}C$). For the same compound but with much bulkier counter ions we reported microphase separation (after prolonged annealing of the melt) with a lamellar period of about 12 nm [14]. The larger value found here indicates considerable stretching of the chains, as expected upon crystallization. From the single X-ray peak at q_1^* we cannot unambiguously confirm the block structure to be lamellar. However, from the AFM picture, as well as from the lamellar structure observed both in Ref. [14] and in PEO-PS block copolymers with the same volume ratio and higher molecular mass, the lamellar morphology seems highly probable.

The question is now how the microphase separation between the PEO and PS blocks affects the MLCs. As q_2^* and $q_3^* = q_2^*\sqrt{2}$ are not related to q_1^*, we attribute these peaks to scattering involving MLC aggregates. In general, a $\sqrt{2}$ relation points to a lattice with cubic or square ordering. In our system each MLC is tethered to two polymer blocks and the possibility of a macrophase separation of the MLCs can be ruled out. Bearing this in mind, cubic packing would lead to incorporation of the MLC aggregates into the lamellae, resulting in fragmented crystallites. The AFM images show this is not the case as rather continuous regular lamellae are observed. On the other hand, any perfect three-dimensional periodic packing of the MLC aggregates is expected to fail because of the unequal thicknesses of the two blocks. As discussed elsewhere [14], amorphous PEO and PS blocks (without any MLCs) have estimated sizes of 1.9 and 2.5 nm, respectively. From these considerations packing of the MLC aggregates in a two-dimensional square lattice parallel to the block interfaces in the amorphous PS blocks seems most plausible. Finally, optical microscope images taken during the isothermal crystallization at various crystallization temperatures (not shown here) showed that uncrystallized regions coexist with the crystals at high crystallization temperatures even after saturation of the X-ray signal. Therefore, the high intensity of q_3^* relative to that of q_2^*, especially at $T_c = 40\,^{\circ}C$ can be understood by considering q_3^* as a the superposition of two peaks, one arising from the ordering of the MLCs due to crystallization and one from the still-uncrystallized regions (supercooled melt) (q_m^*). The same situation appears during a heating scan at high temperatures, Fig. 5. In this case, some of the crystals melt already at these temperatures and in turn this melt contributes to q_3^* through q_m^*. The coexistence of crystalline and not yet crystalline regions for very long times at high temperatures points to a competition that must occur during the crystallization process. High crystallization temperatures lead to thicker lamellae as well as longer long spacings. Consequently, the amorphous PS block is stretched more and more with increasing the crystallization temperature. Progressive stretching of the PS block generates increasing opposing entropic forces. It may also lead to some disassociation of the MLC aggregates. Meanwhile, the thermodynamic driving force for crystallization diminishes with increasing the crystallization temperature. On the other hand, the electrostatic forces responsible for the MLCs aggregation persist at high temperatures. This leads to a tradeoff between crystallization, stretching and segregation of the MLCs resulting in some still-uncrystallized regions at high crystallization temperatures.

On the basis of the above observations, we can model the solid-state crystalline morphology of the PS_{20}-[Ru]-PEO_{70} diblock copolymer as shown in Fig. 6. Isothermal crystallization of the PEO block takes place in a disordered PEO/PS melt in which liquidlike distributed MLC aggregates are microphase separated from the polymer melt [13]. Crystallization induces microphase separation between the two blocks which necessitates some rearrangements of the MLC aggregates. The interdependence between the microphase separation and the rearrangement process of the MLC aggregates can be expected to farther the time over which microphase separation takes place. This might explain the long incubation periods before crystallization sets in. The compact chain packing of the crystalline lamellae drives the MLC aggregates out of the PEO blocks into the amorphous PEO and PS regions. So far this would not require any rearrangement of the MLC aggregates. But as each MLC is connected to a PEO block, the packing of once-folded PEO chains in crystalline lamellae will influence the position of the MLC aggregates. This leads to an in-plane square packing of the aggregates at the PS-PEO interface. The two peaks at q_2^* and q_3^* can

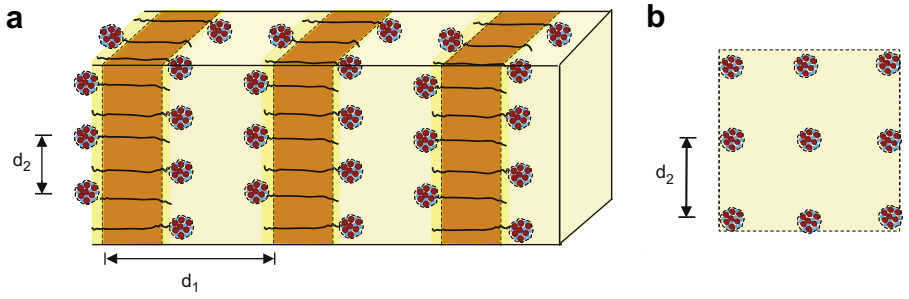

Fig. 6. (a) Schematic drawing of the various regions of isothermally crystallized PS_{20}-[Ru]-PEO_{70}; (b) top-view of the square packing of MLC's at a block interface.

now be assigned as (10) and (11) reflections, respectively in a simple square lattice. The width of any X-ray peak increases with decreasing correlation length or domain size. From the FWHM of the peak at q_2^* (see Table 1) we obtain a typical dimension of the order of 30 nm, comprising approximately four MLC aggregates. Evidently the order of the MLC's in the square lattice is relatively a short-range one. The significant increase of the interlamellar spacing with increasing the crystallization temperature and DSC data, not shown here, indicate that the PEO blocks are not fully crystalline as illustrated in Fig. 6.

Finally we note that after crystallization at 10 °C the MLC peaks are not fully resolved, which, however, can be achieved by a subsequent heating to the melt. This could indicate that the crystalline lamellae formed at low temperatures are less perfect, similarly as known for crystallization of semicrystalline homopolymers. With increasing temperature the crystalline lamellae become better ordered as reflected in the intensity and width of q_1^*. We speculate that the initial crystalline lamellae melt at relatively low temperatures, either partially or completely, subsequently undergo recrystallization and finally melt again around 50 °C (compare Fig. 5b). Such a melting recrystallization is known to be heat rate dependent [25]. The step heating used with a counting time of 600 s for the SAXS curve at each temperature, results in an effectively low heating rate needed to observe such an effect.

5. Conclusions

We have studied the morphology of an isothermally crystallized metallo-supramolecular PS_{20}-[Ru]-PEO_{70} diblock copolymer at different crystallization temperatures. In combination with our earlier work this provides a rather complete insight in the morphological behavior of these materials. In the melt, the PEO and PS blocks are mixed, while the MLC and their associated counter ions form spherical aggregates [13]. For large counter ions only, long annealing leads to a lamellar structure with the MLC aggregates at the PS-PEO block interfaces [14]. For the present small counter ions, crystallization of the PEO block induces microphase separation of the blocks into PEO blocks with crystalline lamellae and amorphous PS blocks. During the crystallization process the MLC aggregates are expelled from the crystalline blocks and redistributed near the interfaces within the amorphous layers. This process result into order of the MLC's in a square lattice parallel to the block interfaces over a relatively short-range. The kinetics of the process depends strongly on the crystallization temperature.

Acknowledgement

We thank B.G.G. Lohmeijer and U.S. Schubert (Dutch Polymer Institute and Eindhoven University of Technology, Eindhoven, The Netherlands) for providing us with the materials. This work is part of the research program of the "Stichting voor Fundamenteel Onderzoek der Materie (FOM)", which is financially supported by the "Nederlandse Organisatie voor Wetenschappelijk Onderzoek (NWO)".

References

[1] Hartgerink JD, Gauba V. Recent advances in supramolecular polymers. New York: Springer; 2007.
[2] Sijbesma RP, Meijer EW. Chem Commun 2003:5.
[3] Ikkala O, ten Brinke G. Science 2002;295:2407.
[4] Antonietti M. Nat Mater 2003;2:9.
[5] Manners I. Science 2001;294:1664.
[6] Meier MAR, Schubert US. Soft Matter 2006;2:371.
[7] (a) Schubert US, Eschbaumer C. Macromol Symp 2001;163:177;
(b) Schubert US, Eschbaumer C. Angew Chem 2002;41:2892.
[8] Bates FS, Fredrickson GH. Annu Rev Phys Chem 1990;41:525.
[9] Hamley IW. The physics of block copolymers. New York: Oxford; 1998.
[10] Park M, Harrison CK, Chaikin PM, Register RA, Adamson DH. Science 1997;276:1407.
[11] Park C, Yoon J, Thomas EL. Polymer 2003;44:6725.
[12] Muthukumar M, Ober CK, Thomas EL. Science 1997;277:1225.
[13] Al-Hussein M, Lohmeijer BGG, Schubert US, de Jeu WH. Macromolecules 2003;36:9281.
[14] Al-Hussein M, de Jeu WH, Lohmeijer BGG, Schubert US. Macromolecules 2005;38:2832.
[15] Lohmeijer BGG, Schubert US. Angew Chem Int Ed 2002;41:3825.
[16] Li L, Sérégo Y, Koch MHJ, de Jeu WH. Macromolecules 2003;36:529.
[17] Zhu L, Cheng SZD, Calhoun BH, Ge Q, Quirk RP, Thomas EL, et al. Polymer 2001;42:5829.
[18] See for example Loo YL, Register RA. In: Hamley IW, editor. Developments in block copolymer science. Chichester: Wiley; 2004.
[19] Mortensen K, Brown W, Almdal K, Alami E, Jada A. Langmuir 1997;13:3635.
[20] Zhu L, Chen Y, Zhang A, Calhoun BH, Chun M, Quirk RP, et al. Phys Rev B 1999;60:10022.
[21] Huang L, Yuan H, Zhang D, Zhang Z, Guo J, Ma J. Appl Surf Sci 2004;225:39.
[22] Kim SH, Misner MJ, Yang L, Gang O, Ocko BM, Russell TP. Macromolecules 2006;39:8473.
[23] Hsiao MS, Zheng JX, Leng S, Van Horn RM, Quirk RP, Thomas EL, et al. Macromolecules 2008;41:8114.
[24] Takahashi Y, Tadokoro H. Macromolecules 1973;6:672.
[25] Al-Hussein M, Strobl G. Macromolecules 2002;35:1672.